Journal of Applied Fluid Mechanics, Vol. 16, No. 9, pp. 1792-1805, 2023.
Available online at www.jafmonline.net, ISSN 1735-3572, EISSN 1735-3645.
https://doi.org/10.47176/jafm.16.09.1715

Cavitation Characteristics and Structure Optimization of Two-Dimensional Valve Based on Entropy Production Theory

Y. Zhao [1,2†], J. Mi[3] and J. Ruan[4]

[1]*Jiaxing Vocational & Technical College，Jiaxing，Zhejiang, 314036, China*
[2]*Jiaxing Key Laboratory of Aero-engine Key Parts Manufacturing Technology, Jiaxing, Zhejiang, 314036, China*
[3]*College of Materials, Lanzhou University of Technology, Lanzhou, Gansu, 730050, China*
[4]*College of Mechanical Engineering，Zhejiang University of Technology，Hangzhou，Zhejiang, 310014, China*

†*Corresponding Author Email: 787077286@qq.com*

ABSTRACT

In addition to noise and vibration, cavitation also lowers the efficiency, performance, and working lives of two-dimensional valves. To study the effect of cavitation on the flow characteristics of two-dimensional valves, standard $k-\omega$ turbulence model and an energy equation model were selected, and the local entropy production rate was defined using the custom field function. The entropy production theory was introduced to numerically simulate the cavitation flow in a two-dimensional valve, and based on this, the structure of the pilot stage of the valve was optimized. The results showed that there was a distinct correlation between the entropy production and the flow characteristics of the valve. When the mass flow rate changed, the entropy production also changed. The turbulent dissipation entropy production always accounted for more than 50% of the total entropy production in the flow field. In the valve sleeve chute area downstream of the valve throttling port, turbulence dissipation entropy production was concentrated; and the energy loss was large. According to the optimization of the structure of this area, the total entropy production of the side-V-slot valve sleeve structure was 7.46% lower than that of the unslotted valve sleeve structure for different valve openings, while the total entropy production of the rear-V-slot valve sleeve structure was 14.31% higher. The energy loss caused by cavitation could be better reduced using a V-shaped groove on the side of the valve sleeve.

Article History

Received December 13, 2022
Revised April 2, 2023
Accepted April 21, 2023
Available online July 1, 2023

Keywords:

Two-dimensional valve
Turbulent dissipation entropy production
Cavitation
Suppression
Computational fluid dynamics

1. INTRODUCTION

The pressure, flow and direction control of the valve was realized by rotating (pilot stage, using the chute on the valve sleeve combined with a high- and a low-pressure holes on the spool to control pressure changes) and axial (power stage, driven by the static force of the fluid) movement of a single spool. Two-dimensional (2D) valves had stability performance and high power/weight ratio, which is a trend of the hydraulic valve lightweight development (Zheng et al., 2021). High-pressure oil forms complex turbulent flow fields, such as jet flows and eddy currents, through the high-pressure valve port of 2D valve, and are accompanied by cavitation (Liang et al., 2022). Cavitation has a significant impact on the flow characteristics of 2D valves and is an important cause of the pressure pulsations, vibrations, and noise of 2D valves (Zhao et al., 2022a,b).

By means of numerical simulations and laboratory analysis, scholars around the world have studied the cavitation location in the valve, the cavitation intensity, and suppression methods considering the valve structure parameters, the opening the throttle orifice of the valve, and the boundary conditions of the inlet and outlet of the valve. The cavitation in a throttle valve extended gradually from the valve hole, which will cause damage to the downstream structure of the valve port (Liu et al., 2022). In an electro-hydraulic servo valve, the first cavitation occurred at the front of the valve flap and at the sharp corner of the nozzle walls. (Li et al., 2013). With a small opening, the cavitation bubble of a high-pressure shrouded valve first appears near the valve port and fades away after some distance (Saito et al., 2007). For globe valves, cavitation usually occurs in the undercarriage of the valve when the opening is small, while cavitation mainly occurs downstream of the valve disc when the opening of the valve is relatively large (Ferrari & Leutwyler, 2008).

Through numerical simulation of reversing globe valves, Lee et al. (2016) found that an increase in the length of the end and middle of the spool resulted in a decrease in cavitation intensity in the valves. Increasing the inlet pressure will lead to an increase in cavitation strength in the valve (Bernad et al., 2007; Ou et al., 2015a; Zheng et al., 2016; Liu et al., 2017). With the increase in the valve opening, the area of the cavitation at the front end of the valve lip of the reducing valve decreases (Ou et al., 2015b), and the cavitation intensity of a pilot type stop valve (Qian et al., 2016) decreases with the increase in the opening of the valve. The cavitation intensity of a rotary valve increases with the decrease of the spool diameter. The cavitation of the valve was suppressed by selecting the appropriate groove depth (Liu & Ji, 2009). Better cavitation resistance of the control valve can be achieved using a chamfered circle, a right conical angle, and a chamfered hole (Wang et al., 2016). Xue et al. (2007) experimentally studied the effect of the throttle port structure on the pressure gradient, cavitation characteristic, and noise of the valve. Xiao et al. (2020) simulated the influence of throttle orifice plate on the cavitation inhibition of compound voltage regulator by Fluent.

It is known from the abovementioned studies that the combination of numerical calculations and laboratory verification can be used to qualitatively analyze the occurrence intensity and suppression methods of cavitation in a valve. Because computational fluid dynamics can obtain more accurate and detailed information about the flow field inside of fluid machinery, some scholars directly determined the flow deteriorating area in the flow field by the analytical theory of entropy production and quantitatively described the energy loss in the flow field through numerical simulations.

On the basis of minimizing entropy production, some researchers (Bejan & Kestinj 1982; Kock & Herwig, 2004; Herwig & Kock, 2007) computed a time average of the entropy generation transport equation. By comparison of the advantages and disadvantages of the direct method and the indirect method to calculate the entropy generation in a convective heat transfer problem, it was confirmed that the direct method has higher accuracy. Zhang et al. (2017) applied the entropy generation method to evaluate the energy consumption of the centrifugal pump and compared the results with the traditional hydraulic performance evaluation results to confirm the feasibility of applying the local entropy generation method to the energy consumption evaluation of the centrifugal pump. Li et al. (2018) analyzed the head fracture characteristics of a centrifugal pump caused by cavitation with the theory of entropy production and found that there was a correlation between the variation trend of the entropy production and the variation trend of the external characteristics of the centrifugal pump. Through numerical analysis of the flow field around the 2D NACA0009 hydrofoil, Zhang et al. (2019) showed that when the lift coefficient and drag coefficient suddenly changed, entropy production and energy loss also changed dramatically, and the energy loss was always concentrated at the end of the hole. Gong et al. (2013) used entropy production theory to analyze the hydraulic loss of large Francis turbines, and the results showed that entropy production theory could accurately locate the high loss position. When entropy generation theory was used to analyze a low-temperature submersible pump of liquefied natural gas (Hou et al., 2016; Wang et al., 2019), the key factors of energy loss in the submersible pump were obtained, indicating that entropy generation theory can also be effectively applied in complex flow fields. Pei et al. (2016) used entropy production theory to evaluate the energy loss caused by the axial clearance between the impeller and diffuser cascade in a water pump, and the results showed that turbulent dissipation was the key factor to hydraulic loss. Wang et al. (2011) applied entropy generation theory to optimize the impeller of a centrifugal fan, improve the flow in the impeller, and improve the performance of the fan.

Research on the suppression of turbulent dissipation has mainly focused on the reduction of wall friction resistance. Many scholars have reached a consensus that a micro-groove structure can reduce the surface friction on a turbulent wall (Walsh 1983; Bacher & Smith, 1986; Pollard & Savill, 1996; Ji et al., 2004; Liu, 2008; Lee & Choi, 2008; Li, 2019), and the research and application on drag reduction technology are still ongoing. Bechert & Bartenwerfer (1989) pointed out that reducing the span-wise velocity fluctuations in the coastal area is helpful for reducing the drag. Choi et al. (1993) conducted direct numerical simulations (DNSs) of turbulent channel flows with fully developed 2D ribs and concluded that drag reduction ribs reduced velocity fluctuations in terms of the root mean square (RMS)near the ribs, and they discussed the relationship between the drag reduction effect and the vortex structure. Chu & Karniadakis (1993) and Goldstein et al. (1995) further proved that the interactions between the inhibition of large-scale turbulence and the surface area of the drag reduction ribs could reduce the areas of high-shear stress and the RMS velocity fluctuations near the drag reduction ribs. In terms of the determination of micro-groove parameters, Cong and Feng (2006) verified the precision and reliability of drag reduction of the non-smooth surface of a groove through numerical simulations of the flow field on surfaces with 26 kinds of triangular grooves, and they provided a method to determine the parameters of these grooves. Song et al. (2009) calculated the corresponding relationship between the accompanying wave width-to-height ratio and the drag reduction of V-shaped grooves inside pipelines with different fluid speeds, and they concluded that the drag reduction would be enhanced with the increase in the accompanying wave width-to-height ratio under the same height condition. Liu et al. (2020) also analyzed the entropy production in the flow process of a plate with a groove and studied the variation of the entropy generation caused by the groove structure. The results showed that the groove structure could decrease the entropy production in the flow process, and the conclusions provided a theoretical basis for optimizing the drag reduction with the groove structure.

In conclusion, it was an effective means to analyze the flow field of hydraulic components qualitatively and quantitatively based on entropy production theory, but it had not been reported in hydraulic valves. In this paper, the entropy production theory was introduced into the

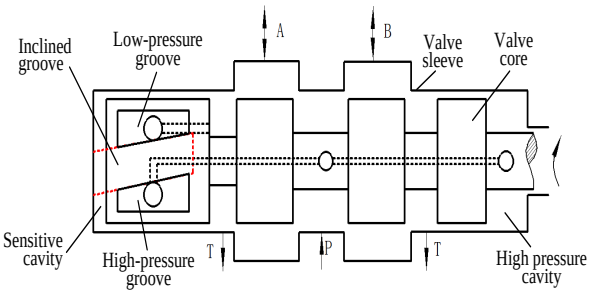

Fig. 1. 2D valve schematic diagram.

flow field analysis of the 2D valve, the influence of cavitation on the 2D valve performance was quantitatively studied, and the size and location of the energy dissipation were accurately determined. Then the structure of the valve was optimized by combining micro-slot drag reduction technology, to achieve the purpose of restraining cavitation and turbulent dissipation in the valve. The results can provide a useful reference for the structural optimization and cavitation suppression of 2D valves.

2. PHYSICAL MODEL AND CALCULATION METHOD

2.1 Physical Model

The 2D valve schematic diagram was shown in Fig. 1. When the driven valve spool rotated, the overlapping area of the high- and low-pressure ports on the valve sleeve was changed, which changed the pressure of the sensitive chamber, and finally drove the valve spool to move axially and output pressure and flow. The main parameters of the 2D valve are shown in Table 1.

The model of 2D valve was built with NX, and the pilot runner of the valve was taken as the research object (Fig. 2(a)). Because of its symmetrical structure (Fig. 2(b)), half of the model was taken for grid division. The

Table 1 Main parameters of 2D valve

Parameter	Value
Operational parameters	
Rated flow rate(L/min)	3.5
Output flow(L/min)	2
Rated pressure(MPa)	35
Pressure difference(MPa)	3.5
Current flow ratio	0.3
Valve core speed(r/s), n	1.047
Geometrical parameters	
Valve core diameter(mm)	6
Area Gradient(mm)	6.28
Valve core and sleeve clearance(um)	3
Maximum opening equivalent diameter(mm)，h	0.3

fluid in the valve flowed from the spool through the throttling orifice to the valve sleeve. The inlet and outlet of the model were shown in Fig. 2 (c). The center of the inlet cross section of the fluid model was taken as the origin of the coordinate system.

2.2 Calculation Method

The numerical calculation was carried out under isothermal conditions. The mixture variable was defined by the mixture model. The mixture conservation equation was applied to model the mixture. The governing equation is as follows:

$$\frac{\partial \rho_m}{\partial t}+\frac{\partial\left(\rho_m u_j\right)}{\partial x_j}=0 \tag{1}$$

$$\frac{\partial\left(\rho_m u_i\right)}{\partial t}+\frac{\partial\left(\rho_m u_i u_j\right)}{\partial x_j}=-\frac{\partial p}{\partial x_i}+\frac{\partial}{\partial x_j}\left[\left(\mu+\mu_t\right)\left(\frac{\partial u_i}{\partial x_j}+\frac{\partial u_j}{\partial x_i}-\frac{2}{3}\frac{\partial u_i}{\partial x_j}\delta_{ij}\right)\right] \tag{2}$$

where u is the mixed medium velocity , p the mixed medium pressure, μ the laminar viscosity coefficient, μ_t the turbulent viscosity coefficient, ρ_m the mixed phase density. The transport equation of the gas phase is as follows:

$$\frac{\partial}{\partial t}\left(\alpha\rho_v\right)+\nabla\cdot\left(\alpha\rho_v u\right)=m^+-m^- \tag{3}$$

$$\rho_m=\rho_v\alpha_v+\rho_l\left(1-\alpha_v\right) \tag{4}$$

where ρ_v is the gas phase density, ρ_l the liquid phase density, α_v the gas phase volume fraction， m^+ and m^- the mass transfer during phase change of liquid and vapor, representing the effects of evaporation and condensation respectively.

The Zwart–Gerber–Belamri (ZGB) cavitation model is chosen to predict cavitating flow:

$$m^+=C_e\frac{3\alpha_{nuc}\left(1-\alpha_v\right)\rho_v}{R_B}\left(\frac{2}{3}\frac{\left|P_v-P\right|}{\rho_l}\right)^{1/2} \tag{5}$$

$$m^-=C_c\frac{3\alpha_v\rho_v}{R_B}\left(\frac{2}{3}\frac{\left|P_v-P\right|}{\rho_l}\right)^{1/2} \tag{6}$$

where R_B is the bubble radius; P_v the saturated vapor pressure, α_{nuc} is the bubble volume fraction, constants C_e = 50, C_c =0.01 (Zhang et al., 2019).

The standard $k-\omega$ model is used for the turbulence model, and the turbulence kinetic energy k and the specific dissipation rate ω are obtained from the following transport equations:

$$\frac{\partial(\rho k)}{\partial t}+\frac{\partial\left(\rho k u_j\right)}{\partial x_j}=\frac{\partial}{\partial x_j}\left[\Gamma_k\frac{\partial k}{\partial x_j}\right]+G_k-Y_k+S_k \tag{7}$$

$$\frac{\partial(\rho\omega)}{\partial t}+\frac{\partial\left(\rho\omega u_j\right)}{\partial x_j}=\frac{\partial}{\partial x_j}\left[\Gamma_\omega\frac{\partial\omega}{\partial x_j}\right]+G_\omega-Y_\omega+S_\omega \tag{8}$$

$$\mu_t=\rho\frac{k}{\omega} \tag{9}$$

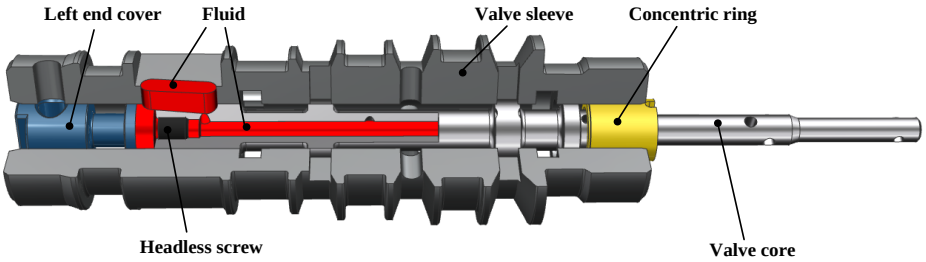

(a) 3D model of 2D valve

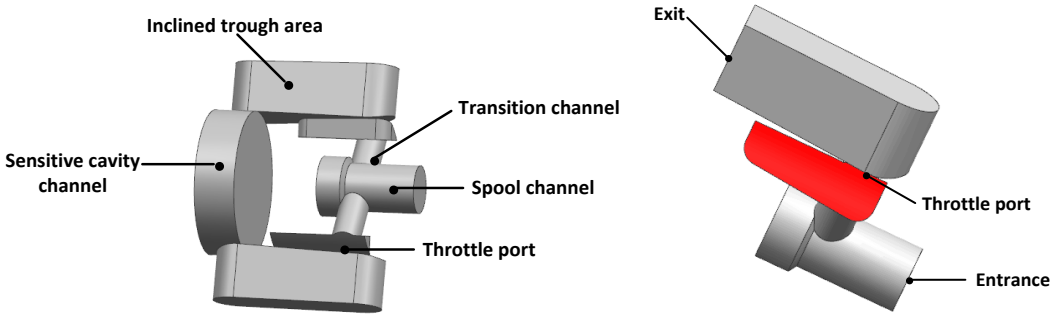

(b) Fluid model (c) Simulation model

Fig. 2. 2D valve model and fluid model.

Where G_k represents the generation of turbulence kinetic energy due to mean velocity gradients. G_ω the generation of ω. Γ_k and Γ_ω the effective diffusivity of k and ω respectively. Y_k and Y_ω the dissipation of k and ω due to turbulence. All of the above terms are calculated as described below. S_k and S_ω are user-defined source terms.

By the second law of thermodynamics, entropy production, an important parameter to irreversible energy loss, is the inevitable result of dissipation effects in the energy conversion process. Referring to Bejan & Kestinj (1982), entropy production per unit volume in the cell during fluid flow and temperature difference heat transfer $\dot{S}'''_{gen}$ can be written as

$$\dot{S}'''_{gen} = \frac{\Phi}{T} + \frac{\Phi_\Theta}{T^2} \tag{10}$$

where Φ is the viscous dissipation function, Φ_Θ is the dissipation term generated by temperature difference heat transfer, T is the temperature.

In Eq. (10), the right-side first term is the entropy generation caused by the dissipation in the flow process, the right-side second term is the entropy generation caused by the heat transfer. In terms of hydraulic machinery, heat transfer effects can be omitted (Fei et al., 2022), and then the specified entropy production rate can be written as follows:

$$\dot{S}'''_{gen} = \frac{\Phi}{T} \tag{11}$$

Here, $\dot{S}'''_{gen}$ includes two parts: one is caused by direct dissipation($\dot{S}'''_{gen,\bar{D}}$) and anotheris caused by velocity fluctuations($\dot{S}'''_{gen,D'}$). $\dot{S}'''_{gen,\bar{D}}$ is induced by the time-averaged velocity and $\dot{S}'''_{gen,D'}$ is induced by turbulent dissipation. The local entropy production rate can be calculated as follows (Kock & Herwig, 2004):

$$\dot{S}'''_{gen} = \dot{S}'''_{gen,\bar{D}} + \dot{S}'''_{gen,D'} \tag{12}$$

$$\dot{S}'''_{gen,\bar{D}} = \frac{\mu}{T}\left\{\begin{array}{l} 2\left[\left(\frac{\partial \bar{u}}{\partial x}\right)^2 + \left(\frac{\partial \bar{v}}{\partial y}\right)^2 + \left(\frac{\partial \bar{w}}{\partial z}\right)^2\right] \\ + \left(\frac{\partial \bar{u}}{\partial y} + \frac{\partial \bar{v}}{\partial x}\right)^2 + \left(\frac{\partial \bar{u}}{\partial z} + \frac{\partial \bar{w}}{\partial x}\right)^2 + \left(\frac{\partial \bar{v}}{\partial z} + \frac{\partial \bar{w}}{\partial y}\right)^2 \end{array}\right\} \tag{13}$$

$$\dot{S}'''_{gen,D'} = \frac{\mu}{T}\left\{\begin{array}{l} 2\left[\left(\frac{\partial u'}{\partial x}\right)^2 + \left(\frac{\partial v'}{\partial y}\right)^2 + \left(\frac{\partial w'}{\partial z}\right)^2\right] \\ + \left(\frac{\partial u'}{\partial y} + \frac{\partial v'}{\partial x}\right)^2 + \left(\frac{\partial u'}{\partial z} + \frac{\partial w'}{\partial x}\right)^2 + \left(\frac{\partial v'}{\partial z} + \frac{\partial w'}{\partial y}\right)^2 \end{array}\right\} \tag{14}$$

However, $\dot{S}'''_{gen,D'}$ being unable calculated in the numerical simulation using the Reynolds averaged Navier-Stokes method but it can be calculated (Kock & Herwig, 2004) as below:

$$\dot{S}'''_{gen,D'} = \beta * \frac{\rho\varepsilon}{T} \tag{15}$$

where ε is the turbulence eddy dissipation.

As mentioned by Zhang et al. (2011), the entropy production rate induced by the wall($\dot{S}'''_{gen,W}$) can be calculated as:

$$\dot{S}'''_{gen,W} = \frac{\tau_W . u_P}{T} \tag{16}$$

Table 2 Calculation conditions

Type	Settings/Options
Primary phase	Hydraulic oil
Density(kg/m^3)	780
Viscosity(kg/m·s)	0.0024
Secondary phase	Air
Density(kg/m^3)	1.225
Viscosity(kg/m·s)	1.789×10^{-5}
Phase interaction	Cavitation
Inlet pressure (MPa)	18
Outlet pressure (MPa)	0.1
Phase flow model	Mixture
Turbulence model	Standard $k-\omega$
Cavitation model	ZGB
Inlet condition	Pressure-inlet
Outlet condition	Pressure-outlet
Pressure-Velocity coupling	Coupled
Method of difference	First order upwind
Temperature (°C)	20

Where τ_W is the wall shear stress and u_P is the velocity at the center of the first grid close to the wall.

The total entropy production $\dot{S}_{gen}$ can be obtained as

$$\dot{S}_{gen} = \int_V \dot{S}'''_{gen,\bar{D}} dV + \int_V \dot{S}'''_{gen,D'} dV + \int_S \dot{S}'''_{gen,W} dS \tag{17}$$

2.3 Boundary Conditions

According to the actual working condition requirements, the calculation conditions are listed in Table 2.The dynamic grid model is adopted. In numerical calculation, the convergence accuracy is set to 0.00001, the time step is set to 0.00005 s, and the calculation is 5000 steps, transient.

The cavitation strength in the valves was expressed by the cavitation number (σ). According to Ruan (2000), σ in 2D valve was defined as:

$$\sigma = \frac{p_2}{p_1 - p_2} \tag{18}$$

where p_1 and p_2 are the upstream and downstream pressure of the throttle port respectively, Pa.

2.4 Grid Generation

The MESH module in ANSYS was used to generate the mesh of the internal flow channel of the 2D valve, as shown in Fig. 3(a). Considering the importance of the valve sleeve (Lu et al., 2018), local mesh refinement was carried out around the valve sleeve, the number of boundary layers was set to 15, and the distance of the first layer was adjusted so that $y^+ < 1$, as shown in Fig. 3(b). The analytical method can be found in the studies of Fei et al. (2022) and Zhang et al. (2021). The value of y+ in the calculation was sufficient to capture turbulence details for this study. In the study of mesh independence, the symmetry plane of the spool and the pressure of the calculated outlet were selected as the evaluation parameters of the mesh error. For the working conditions simulated (Long et al., 2020), the parameter values of the five grids are listed in Table 3. The average pressure values of the symmetry surface of the spinner of mesh 4 and mesh 5 varied within 1.5%, and the average pressure value of the outlet of the valve sleeve varied within 1%, which met the requirement of grid independence. Therefore, grid 4 was adopted in this study for numerical calculations. In other words, the number of grid elements in the studied flow channel using grid 4 was sufficient for the simulations.

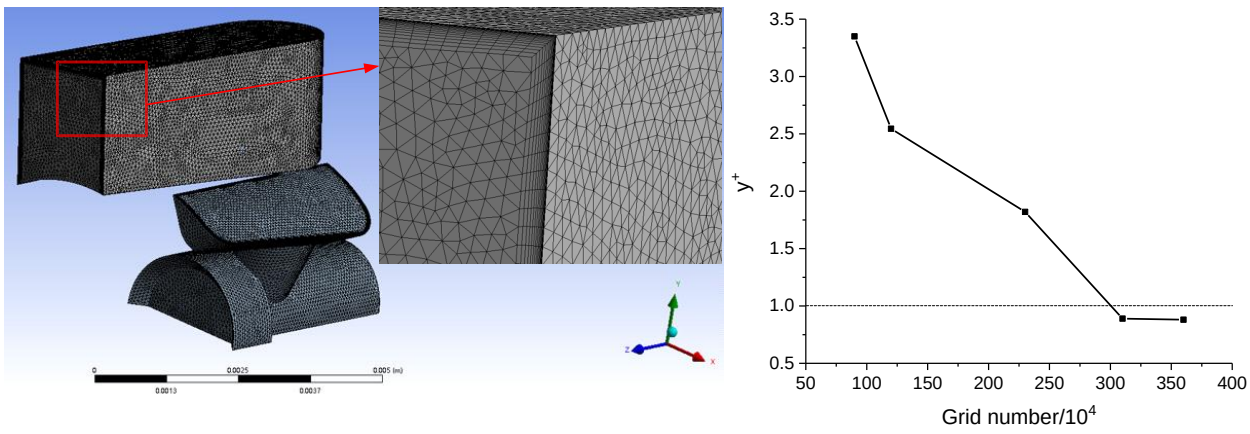

(a) Grid (b) Verification of y+

Fig. 3. Grid and verification of y^+.

Table 3 Grid independence verification

Grid type	Grid number	Sym /Pressure		Outlet /Pressure	
		value(MPa)	Error (%)	value(MPa)	Error (%)
Grid 1	933083	11372800	5.23	94897.2	5.1
Grid 2	1293952	11429200	4.76	96964.35	3.03
Grid 3	2339195	11590700	3.41	97302.39	2.7
Grid 4	3112866	11844000	1.3	99086.59	0.91
Grid 5	3688094	11848500	1.26	99468.72	0.53

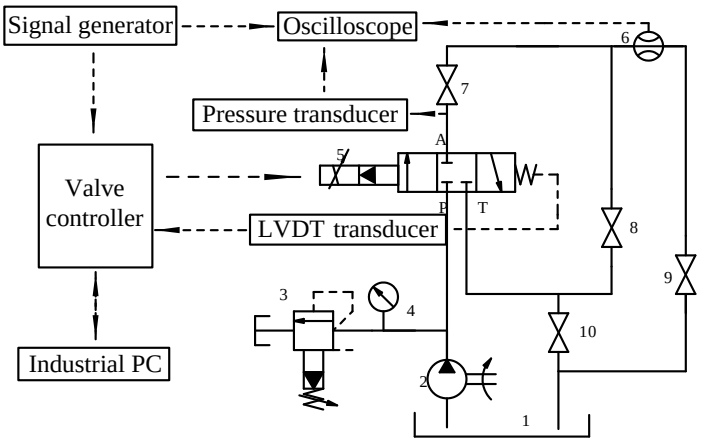

1-Tank 2-Hydraulic pump 3-overflow valve
4-Pressure gauge 5- 2D Cartridge pressure valve
6-Flow meter 7~10-Stop valve
(a) The schematic diagram of the experimental system

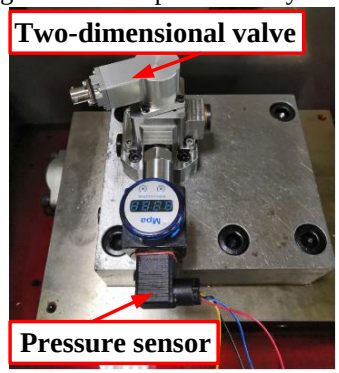

(b) Test platform

Fig. 4. Schematic diagram of the experimental system and test platform.

2.5 Verification of Numerical Simulation

The numerical simulation results were verified on the 2D valve test bench in the Provincial Key Laboratory of Zhejiang University of Technology (Fig. 4). The experimental system was mainly divided into a hydraulic system and an electric control system. The hydraulic system included a hydraulic pump station and a 2D valve to be tested. The electronic control unit included a displacement sensor (model: CD375, measuring range: ±0.63 mm, accuracy: ±3 μm), a pressure sensor (model: CYYZ11, measuring range: 0–40 MPa, precision: 0.1 MPa), 2D valve controller, an oscilloscope, a signal generator, and an industrial computer.

When the system pressure was 18 MPa, a certain voltage signal was input, and the pressure of port A was steady at 10 MPa within 500 s. Figure 5 shows the pressure variation curves of the experimental and computer simulations under no cavitation conditions, and the variation trend was consistent. Due to the influence of the 2D valve on the pressure change in the process of the valve opening changing, in addition to the pilot part studied in this work, the movement of the main spool also had an influence (Lu et al., 2018; Long et al., 2020), and the pressure change amplitude of the numerical simulation was slightly lower than that of the experiment. Therefore, the influence of cavitation on the valve performance could be reliably predicted by numerical simulations.

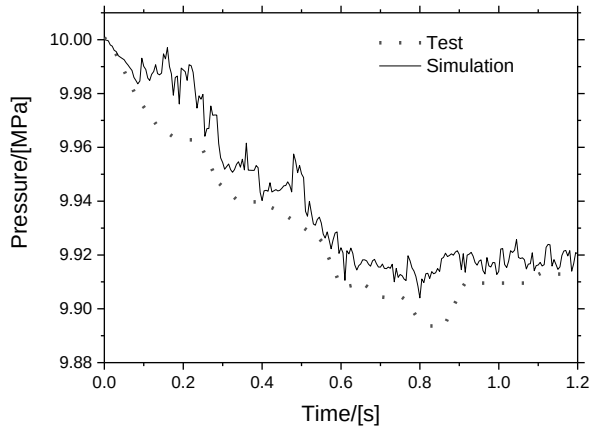

Fig. 5. Verification of numerical simulation.

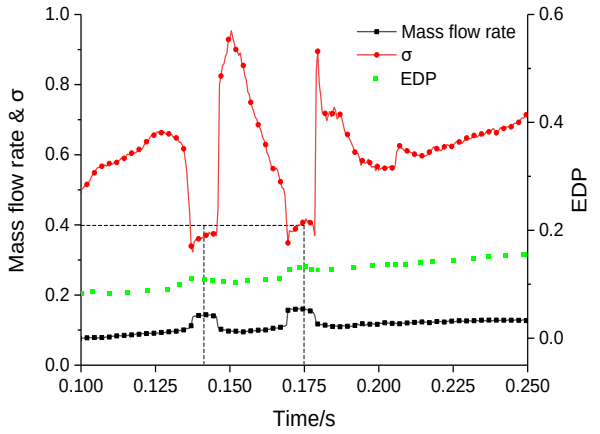

Fig. 6. Variation curves of entropy production and mass flow rate in time-domain.

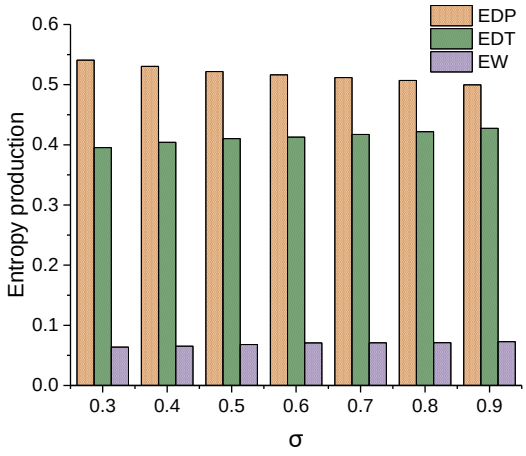

Fig. 7. The proportion of three kinds of entropy production under different cavitation numbers.

3. CALCULATION RESULTS AND DISCUSSION

3.1 Entropy Production and Flow Characteristics

Figure 6 shows the variation of the 2D valve mass flow rate intime domain. The mass flow rate changed dramatically in two strong cavitation periods when the cavitation number was lower than 0.4 (approximately 0.138 s and 0.175 s). In the period when the cavitation number was higher than 0.4, the mass flow rate was relatively steady, indicating that the generation of cavitation had a significant impact on the stability of 2D valve flow rate. In other words, the greater the degree of cavitation, the greater the fluctuation of mass flow rate, and the weaker the cavitation degree, the steadier the mass flow rate. In the time-domain variations shown in Figure 6, the curve of the turbulent entropy generation fluctuated significantly in two strong cavitation periods when the cavitation number was lower than 0.4. This showed that both the entropy production and mass flow rate changed under cavitation conditions.

3.2 Entropy Production Distribution and Flow Field Structure

To analyze the distribution of the entropy production in the flow field, the amounts of three types of entropy production in the flow field were compared first. Figure 7 shows the proportions of three types of entropy generation to the total entropy production for different cavitation numbers. In the figure, turbulence entropy production is represented by EDP, time-mean entropy production is represented by EDT, and wall entropy production is represented by EW. It can be seen that in different cavitation numbers, the proportion of the turbulence entropy generation was greater than 50%, and it was always the greatest component of the total entropy generation. This indicated that the energy change of the pilot stage of the 2D valve mainly depended on the turbulence entropy generation caused by the turbulent dissipation of flow field in the valve. The second was the time-mean entropy generation, which accounted for more than 40% of the total entropy generation. Combined with the results mentioned by Zhao et al. (2022a), the pulsation dissipation in turbulent motion is usually larger than the time-homogeneous dissipation term, which proved the reliability of the entropy generation calculation model adopted in this paper. In the entropy production shown in Fig. 7, the proportions of the wall entropy production at different valve opening degrees were all around 7%, indicating that wall entropy production could not be ignored in the study. The abovementioned analysis showed that turbulent entropy production always played a dominant role in the total entropy production. Therefore, the distribution of turbulent dissipation entropy production in the flow field will the focus of subsequent analysis.

A high-speed jet from a throttle orifice can significantly influence the main flow in the chute area of a valve sleeve (Zhao et al., 2022a). To study the development of cavitation in this region along the flow and spread directions of the fluid, the position and direction of valve sleeve structure optimization were considered，and the section y=4.7 mm was taken as the visualized research object by referring to related works (Zhao et al., 2022b). Figure 8 shows the cloud diagram of gas volume fraction distribution at y = 4.7 mm section in the valve sleeve chute area with different cavitation numbers. With the decrease in the cavitation number, cavitation gradually developed downstream. Figure 9 shows the velocity vector diagram at y = 4.7 mm section of the valve sleeve chute area in different cavitation

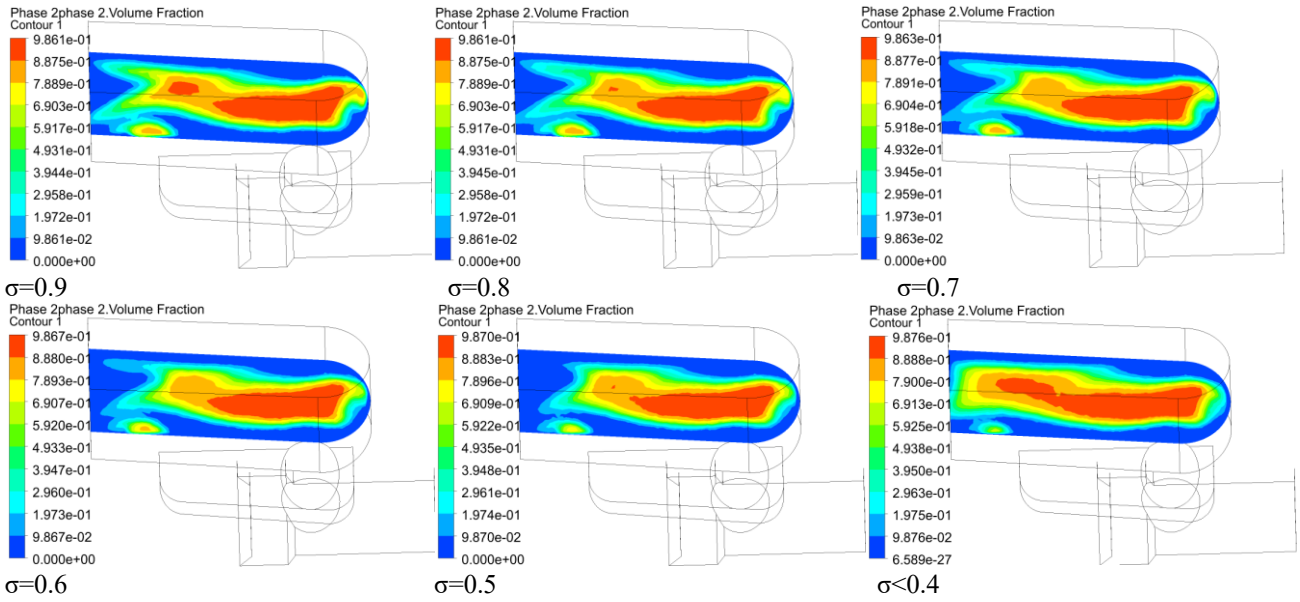

Fig. 8. Cloud map of gas volume fraction distribution at y=4.7mm.

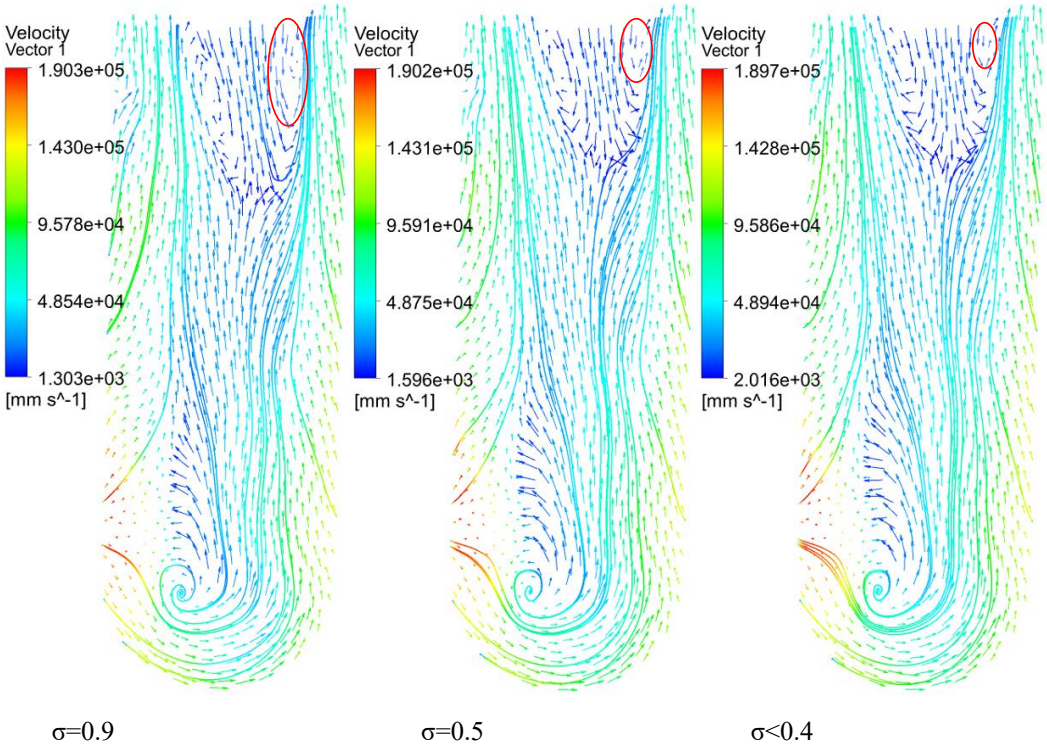

Fig. 9. Velocity vector distribution on the section with different cavitation numbers y=4.7mm.

numbers. It can be seen from the vector arrow direction in Fig. 9 that when the cavitation number was 0.9, a backflow zone at the outlet was significant. By comparing the mass flow rate change curve in Fig. 6, it can be seen that the backflow area weakened the cavitation flow, which was conducive to the flow stability in the valve. Therefore, when the cavitation number was large, the mass flow rate was steady. As shown in Fig. 9, with the decrease in the cavitation number, the backflow area at the outlet gradually decreased, especially the change in the area marked by the red ellipse in Fig. 9. The backflow weakening trend was clear, which is why the mass flow rate fluctuated when the cavitation number was less than 0.4, as shown in Fig. 6.

Figure 10 shows the distribution of turbulent dissipation entropy production (EDP) for different cavitation numbers. With the decrease in the cavitation number, the EDP distribution range near the valve port was basically steady, while the EDP distribution range in the area above the valve sleeve chute and the area outside the valve port gradually increased and extended downstream with the direction of the fluid flow. This indicated that the entropy production loss caused by cavitation was mainly concentrated in the upper and

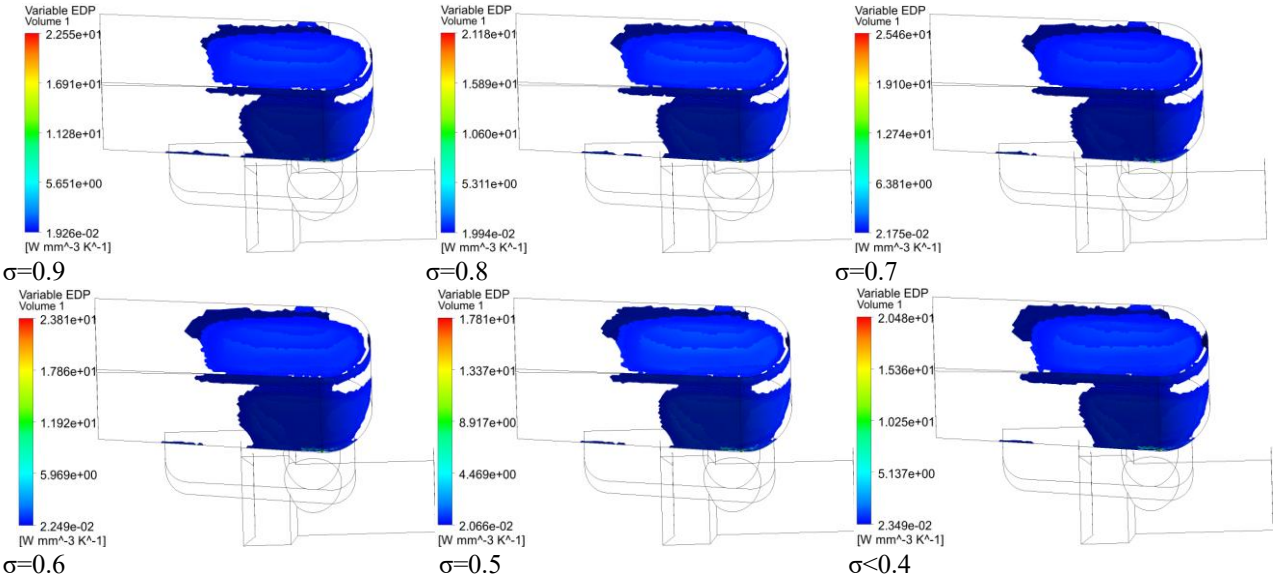

Fig. 10. Distribution of turbulence entropy production with different cavitation numbers.

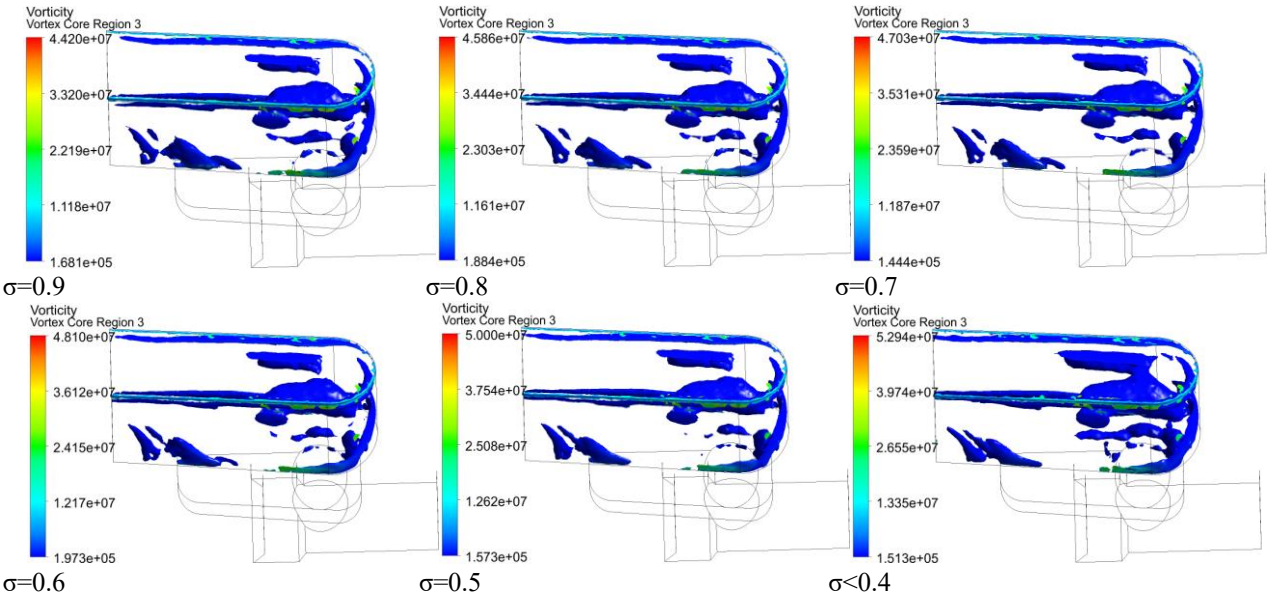

Fig. 11. Vorticity distribution of different cavitation numbers.

outer areas of the valve sleeve chute area. The increase in the cavitation intensity intensified the range expansion of the energy loss areas in flow field, resulting in drastic fluctuations of the mass flow rate at low cavitation numbers.

By comparing distributions of the turbulent dissipation entropy production rate in Fig.10 with the curve of the 2D valve mass flow rate in the time domain in Fig. 6, it was found that the distribution range of the EDP in the chute area of the valve sleeve was closely related to the change of the mass flow rate. When the cavitation number was greater than 0.4, the distribution range of the EDP was basically steady, and the variation of the mass flow rate was steady. When the cavitation number was less than 0.4, the distribution range of the EDP expanded along the direction of fluid flow, and the curve of the mass flow rate fluctuated greatly.

In addition to the jet, the complex flow of eddy was also accompanied by cavitation (Liang et al., 2022). Figure 11 shows the cloud map of the vorticity distribution in the vortex core area (represented by Q-criterion isosurface level of 0.05) in the valve sleeve chute area with different cavitation numbers. By comparing the distribution cloud diagrams of the turbulent dissipation entropy production in Fig. 10, it can be seen that the vortex distribution was larger in the upper part of the valve sleeve chute area where the local turbulent dissipation entropy production was larger. When the cavitation number was less than 0.4, the vorticity in the upper part of the valve sleeve chute area accumulated, and the distribution range was significantly higher than that of the distributed vorticity area when the cavitation number was greater than 0.4. This indicated that the eddy current was accompanied by cavitation, resulting in greater energy loss in this region.

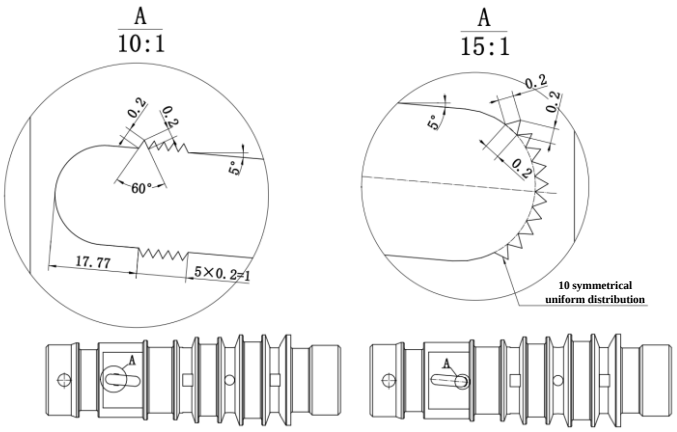

Fig. 12. V-slot position in the valve sleeve chute area.

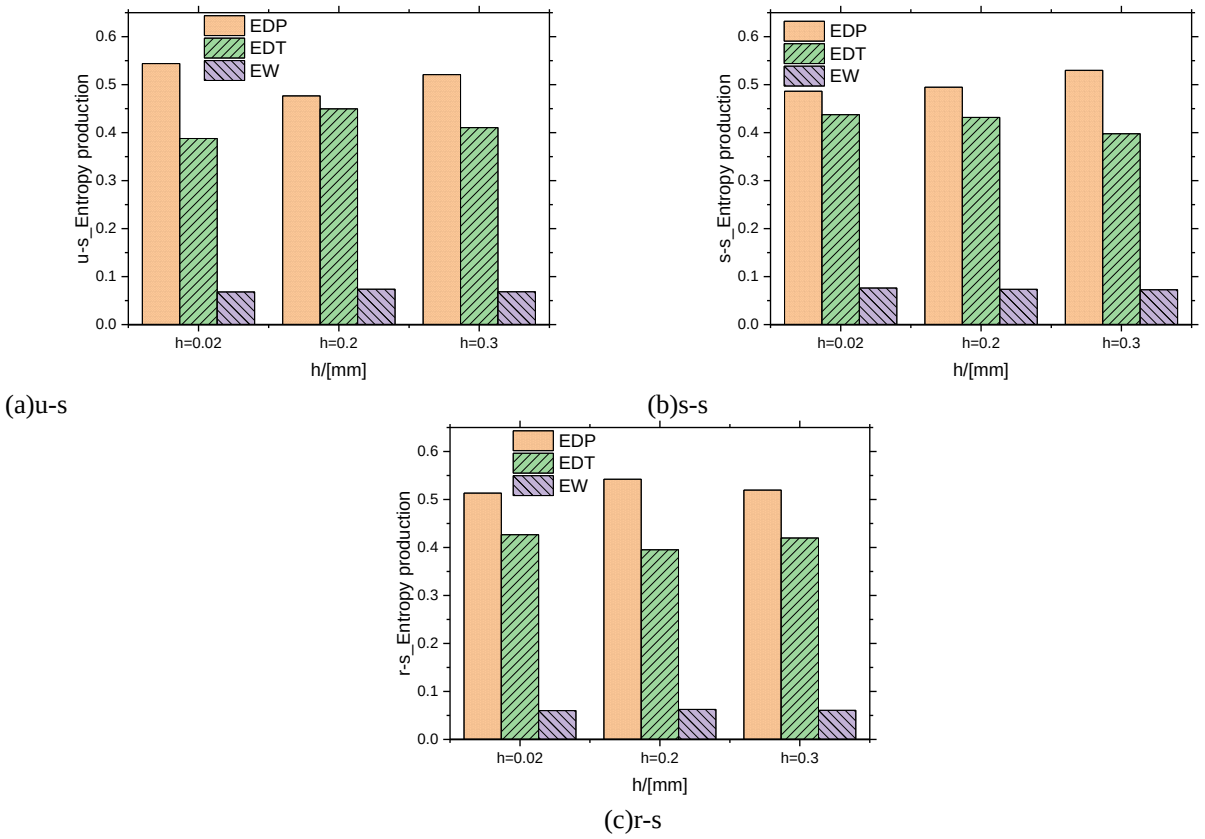

Fig. 13. Proportion of three kinds of entropy production at different structures and valve opening degrees.

Through the abovementioned analysis, it can be concluded that the entropy production distribution can be used as a means to quantitatively study the cavitation degree in the 2D valve flow field. The structure of the 2D valve will be optimized based on the entropy production.

4. STRUCTURAL OPTIMIZATION

4.1 Valve sleeve Structure Optimization

According to the calculation method of the groove parameters provided by Cong and Feng (2006), the cavitation suppression structure of the V-shaped groove opening in the chute area of the valve sleeve of the 2D valve was determined in this study. Based on the structural characteristics and functional requirements of the 2D valve, the structure and slot position of the slotted valve sleeve are shown in Fig. 12, and V-shaped slots were opened on the side and back of the valve sleeve.

4.2 Analysis of Entropy Generation of V-Groove Structure

The valve opening during the operation of the 2D valve was selected as the study condition (Long et al., 2020). The equivalent diameter *h* of the study valve opening (hereinafter referred to as the valve opening) was equal to 0.02, 0.2, or 0.3 mm, The ratios of the three entropy generation types to the total entropy generation for the side-slot valve sleeve structure (s-s), the rear-slot valve sleeve structure (r-s), and the unslotted valve sleeve structure (u-s) when the valve was opened at different positions were compared, and the results are shown in Fig. 13.

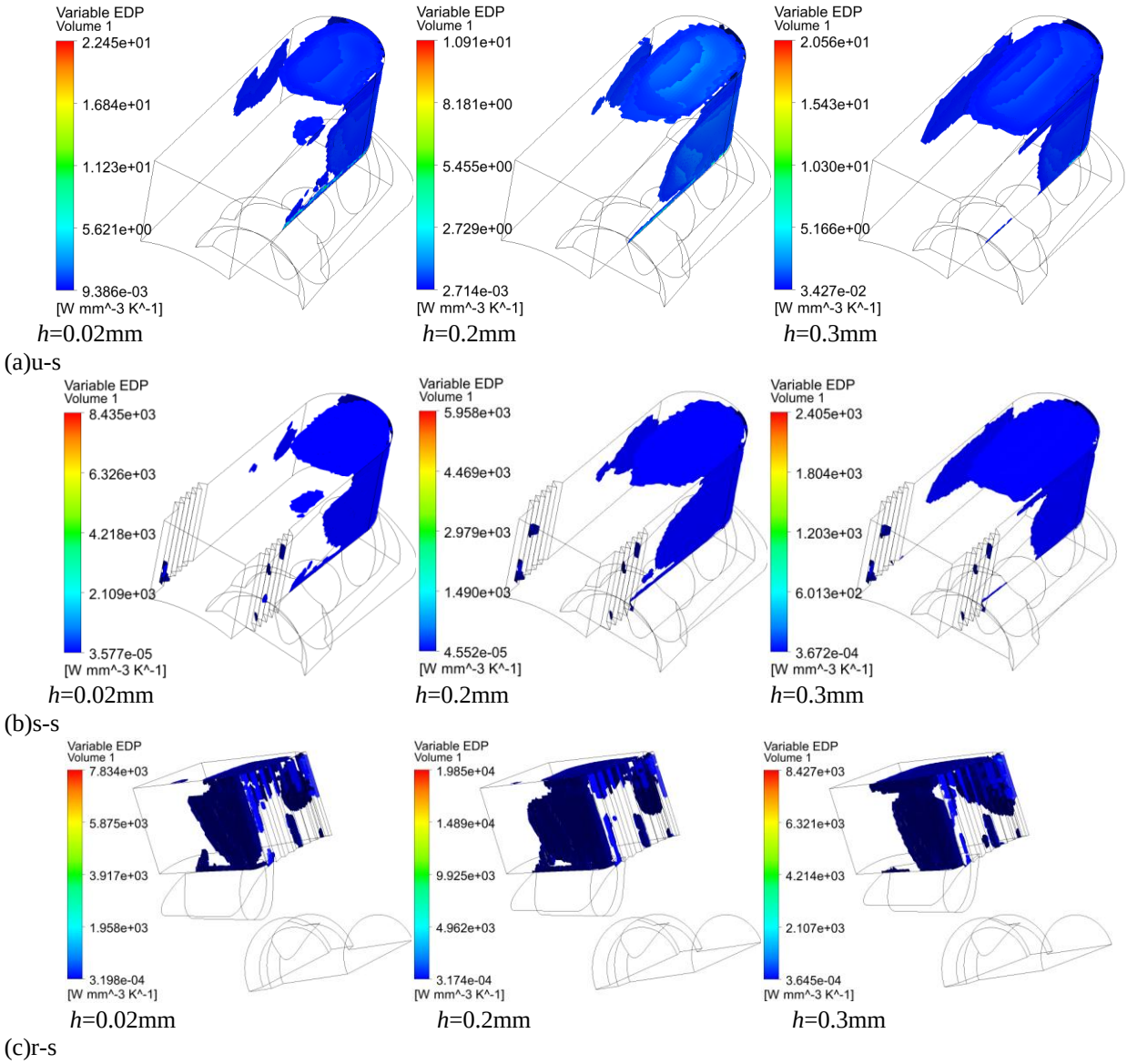

Fig. 14. Distribution of turbulent dissipation entropy production (EDP) at different structures and valve openings.

When the valve opening was 0.02 mm, only the EDP of the side-groove valve sleeve structure was less than 50%, and the EDPs of the other two structures were more than 50%. The EDP of the unslotted valve sleeve structure was closer to 55%, which was higher than that of the rear-groove valve sleeve structure. When the valve opening was 0.2 mm, the EDP ratio of the rear-groove valve sleeve structure was close to 55%, the EDP ratios of the other two structures were less than 50%, and the EDP ratio of the unslotted valve sleeve structure was lower than that of the side-groove valve sleeve structure. When the opening of the valve was 0.3 mm, the EDP ratios of the three structures were greater than 50%. By comparing the ratio of wall entropy production of the three structures, it can be seen that the wall entropy generation ratio of the side-slot valve sleeve structure at the three valve openings was more than 7%.

From the abovementioned analysis, it can be seen that the proportion of turbulent dissipation entropy production to the total entropy production of the structure with the V-groove opening at the side of the valve sleeve was lower than that of the structure without the groove when the opening of the valve port was small. For the structure with the V-groove at the back of the valve sleeve, with the increase in the valve opening, the proportion of turbulent dissipation entropy to the total entropy generation was significantly higher than that of the structure without a groove.

4.3 Distribution of Entropy Production in V- Groove Structure

Figure 14 shows the distribution of turbulent dissipation entropy production (EDP) for three valve sleeve structures with different port openings. When the valve opening was 0.02 mm, the EDP distributions on the inside and upper part of the valve sleeve were not much different for the three kinds of structures, but the EDP distributed on the outside of the valve sleeve was significantly higher than that on the slotted structure. In the rear-slotted structure, the EDP was more distributed than it was in the side-slotted structure. With the opening

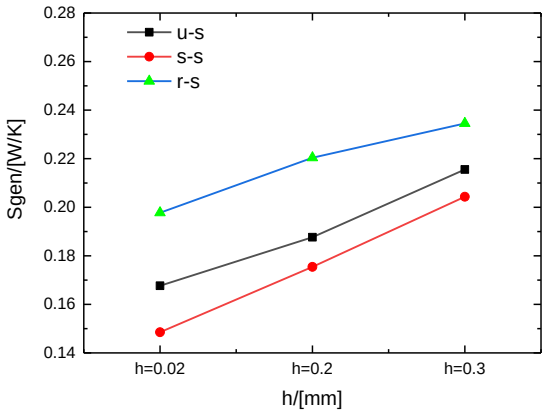

Fig. 15. Comparison of total entropy production rates of three valve sleeve structures with different opening degrees.

of valve port 0.2 mm, the EDP distribution in side-groove valve sleeve structure and the unslotted valve sleeve structure was compared. The results showed that the EDP distribution in the valve sleeve was basically the same, but there was a small amount of EDP distribution in the V-shaped groove of the side-groove valve sleeve structure than that in the unslotted structure. The EDP distribution inside the rear-groove valve sleeve structure extended and converged with the EDP distribution at the throttle port, and the local entropy production increased significantly, indicating that the turbulence degree was intensified at this moment. When the valve opening was 0.3 mm, the EDP distribution of the side-groove valve sleeve structure and the unslotted valve sleeve structure had little difference, and the EDP distribution area inside the rear-groove valve sleeve structure shrank compared with that when the valve opening was 0.2 mm.

Figure 15 shows the comparison of the total entropy production rates of three valve sleeve structures for different valve opening degrees. The total entropy production rate of the side-groove valve sleeve structure was always lower than that of the unslotted valve sleeve structure (the average was 7.46% lower), while the total entropy production rate of the rear-groove valve sleeve structure was always higher (the average was 14.31% higher).

5. CONCLUSION

By using numerical simulations, entropy production theory was applied to analyze the energy loss in the 2D valve cavitation flow field. Based on this, the structure of the 2D valve was optimized, and the following conclusions were obtained:

A distinct correlation between the entropy production and the flow characteristics of the 2D valve exists. When the flow rate changed, the entropy production also changed significantly. Entropy production theory could well explain the relationship between the flow fluctuations of the 2D valve and the development of cavitation, verifying its applicability in the analysis of the cavitation flow field.

In the cavitation flow field, the entropy production induced by turbulent dissipation always accounted for more than 50% of the total and was its dominant source. The valve sleeve chute area downstream of the throttle of the 2D valve was the area where the turbulent dissipation entropy production rate was concentrated and the energy loss was large. This was the area of the pilot stage of the 2D valve mainly targeted for structural optimization.

Entropy production theory intuitively and quantitatively showed the distribution of entropy production loss in the flow field after the pilot stage structure optimization of 2D valve. Through comparison, the study showed that the proportion of turbulent dissipation entropy production to the total entropy production of the side-groove valve sleeve structure was lower than that of the unslotted valve sleeve structure when the valve opening was small. With the valve opening of the V-shaped groove at the rear-groove valve sleeve, the proportion of turbulent dissipation entropy production to the total entropy production was higher than that of the unslotted valve sleeve when the valve opening increased. When three valve ports were open, the total entropy production of the side-V-slot valve sleeve structure was 7.46% lower than that of the unslotted valve sleeve structure for different valve openings, while the total entropy production of the rear-V-slot valve sleeve structure was 14.31% higher. Therefore, the V-groove structure with the side-valve sleeve opening could better reduce the energy loss caused by cavitation.

ACKNOWLEDGEMENTS

The authors would like to thank the support of National Key Research and Development Project (Project No.2019YFB2005201), and the National Natural Science Foundation of China (Project No. 51675482).

CONFLICT OF INTEREST

The authors declare that they have no competing interests.

AUTHOR CONTRIBUTION

Y. Zhao: Conceptualization; Data collection; Visualization; Writing the original draft. J. Mi:Conceptualization (supporting); writing; review and editing. J. Ruan: Supervision, review and editing.

REFERENCES

Bacher, E. V., & Smith, C. R. (1986). Turbulent boundary-layer modification by surface riblets. *American Institute of Aeronautics and Astronautics*, 24(8), 1382-1385. https://doi.org/10.2514/3.48695

Bechert, D., & Bartenwerfer, M. (1989). The viscous flow on surfaces with longitudinal ribs. *Journal of Fluid Mechanics*, 206, 105-129. https://doi.org/10.1017/S0022112089002247

Bejan and Kestinj (1982). *Entropy generation through heat and fluid flow*. John Wiley and Sons, New York, USA.

Bernad, S., Susan, R., & Muntean, S. (2007). Cavitation phenomena in hydraulic valves. *Numerical Modeling Proceeding the Romanian Academy*: *A*, 8(2), 113-124. https://doi.org/10.1299/kikaib.51.427

Choi, H., Moin, P., & Kim, J. (1993). Direct numerical simulation of turbulent flow over riblets. *Journal of Fluid Mechanics*, 225, 503–539. https://doi.org/10.1016/j.ijheatfluidflow.2022.109069

Chu, D., & Karniadakis, G. (1993). A direct numerical simulation of laminar and turbulent flow over riblet mounted surfaces. *Journal of Fluid Mechanics*, 250, 1-42. https://doi.org/10.1017/jfm.2022.393

Cong, Q., & Feng, Y. (2006). Numerical simulation of surface flow field in triangular grooves. *Journal of Ship Mechanics*, 10(5), 11-16. https://doi.org/10.3969/j.issn.1007-7294.2006.05.002

Fei, Z., Zhang, R., & Xu, H. (2022). Energy performance and flow characteristics of a slanted axial-flow pump under cavitation conditions. *Physics of Fluids*, 34(3), 1-21. https://doi.org/10.1063/5.0085388

Ferrari, J., & Leutwyler, Z. (2008, December). *Fluid flow force measurement under various cavitation state on a globe valve model*. ASME Pressure Vessels and Piping Conference, Chicago, Canada.

Goldstein, D., Handler, R., & Sirovich, L. (1995). Direct numerical simulation of turbulent flow over a modeled riblet covered surface. *Journal of Fluid Mechanics*, 302, 333-376. https://doi.org/10.1017/S0022112095004125

Gong, R., Wang, H., & Chen, L. (2013). Application of entropy production theory to hydro-turbine hydraulic analysis. *Science China-Technological Sciences*, 56(7), 1636-1643. https://doi.org/10.1007/s11431-013-5229-y

Herwig, H., & Kock, F. (2007). Direct and indirect methods calculating entropy generation rates in turbulent convective heat transfer problems. *Heat and Mass Transfer*, 50(3), 207-215. https://doi.org/10.1007/s00231-006-0086-x

Hou, H., Zhang, Y., & Li, Z. (2016). Numerical analysis of entropy production on a LNG cryogenic submerged pump. *Journal of Natural Gas Science and Engineering*, 36, 87-96. https://doi.org/10.1016/j.jngse.2016.10.017

Ji, H., Fu, X., & Yang, H. (2004). Experimental study on noise characteristics of throttling groove valve port. *Chinese Journal of Mechanical Engineering*, 40(11), 42-46. https://doi.org/10.1061/(ASCE)AS.1943-5525.0001509

Kock, F., & Herwig, H. (2004). Local entropy production in turbulent shear flows: A high Reynolds number model with wall functions. *International Journal of Heat and Mass Transfer*, 47(10), 2205-2215. https://doi.org/10.1016/j.ijheatmasstransfer.2003.11.025

Lee, M. G., Lim, C. S., & Han, S. H. (2016). Shape design of the bottom plug used in a 3-way reversing valve to minimize the cavitation effect. *International Journal of precision engineering and manufacturing*, 17(3), 401-406. https://doi.org/10.1007/s12541-016-0050-8

Lee, S. J., & Choi, Y. S. (2008). Decrement of spanwise vortices by a drag-reducing riblet surface. *Journal of Turbulence*, 9(23), 23-44. https://doi.org/10.1080/14685240802251517

Li, S. (2019). *TRPIV experimental investigation on drag-reduction mechanism over 2D and 3D riblets*. [Doctoral thesis, Tian Jin University]. Tian Jin, China.

Li, S., Aung, N. Z., & Zhang, S. (2013). Experimental and numerical investigation of cavitation phenomenon in flapper-nozzle pilot stage of an electrohydraulic servo-valve. *Computers & Fluids*, 88, 590-598. https://doi.org/10.1016/j.compfluid.2013.10.016

Li, Y., Feng, G. W., & Si, Q. R. (2018). An experimental study on the cavitation vibration characteristics of a centrifugal pump at normal flow rate. *Journal of Mechanical Science and Technology*, 32(10), 4711-4720. https://doi.org/10.1007/s12206-018-0918-x

Liang, L., Jian, W., & Yang, L. (2022). Numerical simulation analysis of vortex cavitation in spool valve with V-Shape notch. *Hydraulics & Pneumatics*, 46(4), 110-118. https://doi.org/10.11832/j.issn.1000-4858.2022.04.014

Liu, B., Zhao, J., & Qian, J. (2017). Numerical analysis of cavitation erosion and particle erosion in butterfly valve. *Engineering Failure Analysis*, 80, 312-324. https://doi.org/10.1016/j.engfailanal.2017.06.045

Liu, M., Li, S., & Wu, Z. (2020). Analysis of entropy production in a planar flow with grooves. *Journal of Computational Physics*, 37(2), 182-188. https://doi.org/10.19596/j.cnki.1001-246x.8021

Liu, R. (2008). Cavitation of hydraulic system and its prevention measures (2008). *Journal of Tangshan Normal University*, 30(2), 11-17. https://doi.org/10.5293/IJFMS.2022.15.4.401

Liu, X., He, J., & Zhao, J. (2022). Biofluid flow through a throttle valve: A computational fluid dynamics study of cavitation. *Journal of Mechanics in Medicine and Biology*, 16(03), 1650034. https://doi.org/10.1142/S0219519416500342

Liu, Y. H., & Ji, X. W. (2009). Simulation of cavitation in rotary valve of hydraulic power steering gear. *Science in China Series E: Technological Sciences*, 52(11), 3142-3148. https://doi.org/10.1007/s11431-009-0277-z

Long, Q., Ruan, J., & Li, S. (2020). Stability of 2D pressure servo valve considering the influence of cavitation. *Journal of Aeronautics*, 41(5), 1-13. https://doi.org/10.7527/S10006-893.2019.23281

Lu, Q., Ruan, J., & Li, S. (2018). Study on cavitation characteristics of 2D Servo Valve rectangular pilot Control Valve. *Hydraulic and Pneumatic*, 4, 8-14.

https://doi.org/10.11832 /j. issn. 1000-4858. 2018. 04. 002

Ou, G. F., Xu, J., & Li, W. Z. (2015a). Investigation on cavitation flow in pressure relief valve with high pressure differentials for coal liquefaction. *Procedia Engineering*, 130, 125-134. https://doi.org/10.1016/j.proeng.2015.12.182

Ou, G. F., Li, W. Z., & Xiao, D. H. (2015b, May). *Numerical investigation on cavitation in pressure relief valve for coal liquefaction*. International Symposium on Cavitation and *Multiphase* Flow, Beijing, China.

Pei, J., Meng, F., & Li, Y. (2016). Effects of distance between impeller and guide vane on losses in a low head pump by entropy production analysis. *Advances in Mechanical Engineering*, 8(11), 64-88. https://doi.org/10.1177/1687814016679568

Pollard, A., & Savill, A. M. (1996). Simulating turbulent flow over thin element and flat valley v-shaped riblets. *American Institute of Aeronautics and Astronautics*, 34(11), 2261-2268. https://doi.org/10.2514/3.13389

Qian, J., Liu, B., & Jin, Z. (2016). Numerical analysis of flow and cavitation characteristics in a pilot-control globe valve with different valve core displacements. *Journal of Zhejiang University-Science: A*, 17(1), 54-64. https://doi.org/10.1631/jzus.A1500228

Ruan, J. (2000). *Electro-hydraulic (Gas) Direct Digital Control Technology*. Zhejiang University Press, Hangzhou, China.

Saito, S., Shibata, M., & Fukae, H. (2007). Computational cavitation flows at inception and light stages on an axial-flow pump blade and in a cage-guided control valve. *Journal of Thermal Science*, 16(4), 337-345. https://doi.org/10.1007/s11630-007-0337-2

Song, B., Liu, G., & Hu, H. (2009). Simulation study on surface drag reduction of V-Type trailing wave with different aspect ratio. *Computer Engineering and Applications*, 45(32), 222-224. https://doi.org/10.3778/j.issn.1002—8331.2009.32.069

Wang, C., Li, G. X., & Sun, Z. Y. (2016). Effects of structure parameters on flow and cavitation characteristics within control valve of fuel injector for modern diesel engine. *Energy Conversion and Management*, 124, 104-115. https://doi.org/10.1016/j.enconman.2016.07.004

Wang, C., Zhang, Y., & Hou, H. (2019). Entropy production diagnostic analysis of energy consumption for cavitation flow in a two-stage LNG cryogenic submerged pump. *International Journal of Heat and Mass Transfer*, 129, 342-356. https://doi.org/10.1016/j.ijheatmasstransfer.2018.09.070

Wang, S. L., Zhang, L., & Ye, X. M. (2011). Performance optimization generation theory. *Proceedings of the CSEE*, 31(11), 86-91. https://doi.org/10.13334/j.0258-8013.pcsee.2011.11.007

Xiao, K., Xi, H., & Xiu, G. (2020). Optimal design of control valve based on current limiting orifice plate theory. *Journal of Gansu Science*, 532 (6), 78-83. https://doi.org/10.16468/j.cnki.issn1004-0366.2020.06.013

Xue, W., Jun, Z., & Xin, F. (2007). Effect of throttle structure on cavitation noise. *Journal of Zhejiang University (Engineering Edition)*, 41(3), 456-460. https://doi.org/10.3785/j.issn.1008-973X.2007.03.018

Walsh, M. J. (1983). Riblets as a viscous drag reduction technique. AIAA journal, 21(4), 485-486. https://doi.org/10.2514/3.60126

Zhang, H., Zang, J., & Shi, W. (2021). Analysis of the formation mechanism and evolution of the perpendicular cavitation vortex of tip leakage flow in an axial-flow pump for off-design conditions. *Journal of Marine Science and Engineering*, 9(10), 81-98. https://doi.org/ 10.3390/jmse9101045

Zhang, X., Wang, Y., & Xu, X. M. (2011). Energy conversion characteristic within impeller of low specific speed centrifugal pump. *Transactions of the Chinese Society of Agricultural Machinery*, 42(7), 75-81. https://doi.org/10.3969/j.issn.1000-1298.2011.07.015

Zhang, Y. T., Yang, B. F., & Chen, W. (2019). Study on cavitation characteristics of hydrofoil based on entropy production theory. *Journal of Propulsion Technology*, 7, 1490-1497. https://doi.org/10.13675/j.cnki.tjjs. 180467

Zhang, Y. X., Hou, H. C., & Xu, C. (2017). Application of entropy production method to centrifugal pump energy loss evaluation. *Journal of Drainage and Irrigation Machinery Engineering*, 4, 277-282. https://doi.org/10.3969 /j.issn.1674-8530.15.1106

Zhao, Y., Ruan, J., & Ding, C. (2022a). Characteristics of cavitation and pressure fluctuation of a two-dimensional valve based on FLUENT simulation. *Journal of Vibration and Shock*, 41(18), 228-235. https://doi.org/10.13465/j. cnki.jvs. 2022.18.029

Zhao, Y., Ruan, J., & Lu, Q. (2022b). Numerical simulation and mechanism investigations of cavitating noise around a two-dimension valve pilot stage. *International Journal of Acoustics and Vibration*, 27 (1), 10-16. https://doi.org/10.20855/ijav.2022.27.11821

Zheng, F., Li, S., & Ding, C. (2021). Theoretical and experimental research on the cartridge two-dimensional (2D) electro-hydraulic servo valve. *Advances in Mechanical Engineering*, 13(2), 1-12. https://doi.org/10.1177/16878140211015581

Zheng, Z., Ou, G., & Ye, H. (2016, July). *Numerical analysis on cavitation erosion of a high pressure differential control valve*. ASME Pressure Vessels and Piping Conference, Vancouver, Canada.